J. of Fire Prot. Engr., 9 (1), 1998, pp 41-57

AN INTRODUCTION TO A USER-FRIENDLY NUMERICAL FIRE ENDURANCE ALGORITHM

Dee H. Wong, PhD, PE
Advanced Fire Engineering
PO Box 5763
Napa California 94581

ABSTRACT

This paper adopts the simplest numerical procedure for solving the multi-dimensional nonlinear transient heat conduction model, which "occasionally" is used to simulate fire endurance and related fire engineering problems. Due to its superb simplicity, average fire professionals can easily implement this relatively user-friendly algorithm customized for the rarely published fire (convective or Robin) boundary conditions. Further, the danger of *constant incident* (Neumann) flux is discussed. This paper also discusses the cogent investigation of converging solutions, numerical difficulties, comparisons of analytical solutions of a simple benchmark case, and nonlinear problems arising from thermophysical properties, temporal fire including variable combined heat transfer coefficient, and a heat source or sink.

INTRODUCTION

Although numerical fire endurance simulations have existed since the 1970's, e.g., FIRES-T3,[1] the applications are very limited in the general fire community, even in the fire protection consulting engineering industry. It may be partly due to the unawareness of this powerful engineering tool, and partly due to the lack of the knowledge of heat transfer theories or advanced mathematics, i.e., partial differential equations, and the computer programming skills. It is considered imperative that the community be well indoctrinated of the foremost but also the simplest computer modeling, in comparison with the state-of-the-art theoretical fire modeling, such as CFD (Computational Fluid Dynamics) codes coupled with heat and mass transfer and combustion sub-models.

The objective of this paper is threefold. Firstly, it introduces the simplest numerical method; i.e., Explicit Finite Difference Scheme (EFDS), to solve the most common heat conduction model applied to fire endurance simulations. The salient advantage of this scheme is that no complex linear algebra theories and complicated computer programming are involved. It does not even require a grid generator. Other algorithms such as Finite Element and Finite Volume employ advanced mathematical techniques entailing variational calculus, tensor, linear algebra and numerical methods. Even Implicit Finite Difference algorithms would have to utilize some of these techniques. In relation to any of these algorithms, EFDS is indeed "user-friendly." For example, FIRES-T3, based on Linear Finite Elements, cannot be easily understood by an average fire professional. However, in this paper, it is expected that any practicing fire professional, without the background of partial differential equations, can easily follow the numerical procedure, and subsequently will start to simulate some simple yet practical fire endurance problems. It is analogous to that most fire professionals know how to apply the Hardy-Cross Method to network hydraulic models, without the full understanding of numerical analysis and embedded matrix theories.

Secondly, this paper provides some "correct" guidelines for those fire professionals who have already had some experience in this field. Although the generic heat conduction algorithms for prescribed temperature boundary conditions are well publicized in the numerical arena, the convective or radiative flux boundary conditions are rarely published if existent, and are derived

herein specifically for fire endurance applications in the context of both slightly improved numerical accuracy and application versatility.

Thirdly, numerical results of an *ad hoc* numerical benchmark case and a practical example are available for comparison. To promote wider applications of numerical methods or computer modeling in fire protection engineering, numerical results for simple benchmark cases and examples must be available for the community. Focusing on numerical aspects of the computer modeling only, this paper does not address improvements or modifications of the engineering model adopted in the following analysis.

MATHEMATICAL MODEL

Assuming the test or engineering assembly is *completely* solid and pyrolysis does not occur within the assembly, the following heat rate or thermal diffusion equation can be applied to fire endurance simulations,

$$\frac{\partial}{\partial x_j}\left[k\,\frac{\partial T}{\partial x_j}\right] = \rho c_p\,\frac{\partial T}{\partial t} - \dot{q}''' \qquad j=1,\ 2,\ \text{and}\ 3 \tag{1}$$

$\dot{q}'''$ in W/m^3(Btu/(s-ft^3))

where

$T = T(x_j,t)$ = temperature, K (R)
$x_j = x_j(x,y,z) = x_j(x_1,x_2,x_3)$ = Cartesian coordinate vector, m (ft)
t = time, s
$k = k(T)$ = variable thermal conductivity, W/(m-K) (Btu/(ft-s-R))
$\rho = \rho(T)$ = variable density, kg/m^3 (lb$_m$/ft^3)
$c_p = c_p(T)$ = variable specific heat, J/(kg-K) (Btu/(lb$_m$-R))
$\dot{q}'''$ = volumetric heat rate generation, W/m^3 (Btu/(s-ft^3))

To complete Eq (1), three pairs of scalar boundary condition equations are needed for the x, y, and z coordinates. They can be obtained via the following generic *linear* scalar equation,

$$-k\,\frac{\partial T_s}{\partial n} + hT_s = G \tag{2}$$

where

$T_s = T_s(x_j,t)$ = temporal surface temperature at coordinate x_j, K (R)
n = magnitude of outward unit normal vector at boundary, m (ft)
$h = h(x_j,t)$ = constant or variable heat transfer coefficient, W/(m^2-K) (Btu/(s-ft^2-R))
$G = G(x_j,t)$ = constant *or* time-varying nonhomoegenous function for prescribed temperature (Dirichlet), K (R)
or predetermined heat flux (Neumann), W/m^2 (Btu/(s-ft^2))
or zero (homogeneous) function for convection or radiation, or both (Robin), W/m^2 (Btu/(s-ft^2))

If the first term or conductive flux (based on Fourier Law) vanishes and h is unity, then the first kind of boundary condition, which is usually called prescribed temperature (Dirichlet), would result. It equals the nonhomogeneous function $G(x_j,t)$. If the second term or convective flux vanishes, then the second kind of boundary condition, which is usually called prescribed flux (Neumann), would result. It also equals the nonhomogeneous function $G(x_j,t)$. For a common engineering case that both the convective term and $G(x_j,t)$ vanish, adiabatic boundary condition would result, meaning that there is no heat transfer across the boundary. In many practical engineering applications, e.g., CFD fire modeling and thermally-thick-unexposed surfaces of fire compartmentation, the boundary conditions are usually adiabatic in view of the conservative assumption and the great simplification of boundary implementation. Finally, when $G(x_j,t)$ is zero or homogeneous, the last kind of boundary condition is convective or radiative, or both (Robin). In this case, the conductive flux is equal to the convective or radiative flux, or both. It must be emphasized that both the first and second kinds, i.e., prescribed temperature and prescribed flux, can be either constant *or* time-varying, implied by $G(x_j,t)$. However, the third kind of convective type must be time-varying, since the surface temperature under general fire simulations is always a function of time, i.e., $T_s = T_s(x_j,t)$.

Consider the third kind of boundary condition. Rearranging Eq (2) and substituting the normal

vector n_j for a scalar coordinate, the convective boundary condition in the form of Newton's Law of Cooling is

$$\dot{q}''_{cond} = -k\frac{\partial T_s}{\partial x} = \dot{q}''_{conv} + \dot{q}''_{rad} = h_c(T_\infty - T_s) + \dot{q}''_{rad} \quad (3)$$

where

$\dot{q}''_{cond}$ = conductive flux W/m²(Btu/(s-ft²))
$\dot{q}''_{conv}$ = convective flux W/m² (Btu/(s-ft²))
$\dot{q}''_{rad}$ = radiative flux W/m² (Btu/(s-ft²))
T_∞ = known ambient fluid temperature K (R)
T_s = unknown boundary surface temperature K (R)
h_c = assumed convective heat transfer coefficient 25.0 W/(m²-K) (1.22E-3Btu/(s-ft²-R))

In practical fire simulations, radiative heat transfer plays a significant role at the exposed boundaries and therefore cannot be neglected. For simplicity, one of the simplest thermal radiation submodels which is a two-surface gray-diffuse non-enclosure model [e.g., Refs 1–3], is adopted,

$$\dot{q}''_{rad} = VF_{ds\text{-}f}\sigma(\alpha_s\epsilon_f T_f^4 - \epsilon_s T_s^4) \quad (4)$$

where

$\dot{q}''_{rad}$ = radiative flux W/m² (Btu/(s-ft²))
$VF_{ds\text{-}f}$ = view factor from exposed differential boundary to total "visible" 3-dimensional exposing fire surface, dimensionless
σ = Stefan-Boltzmann Constant 5.67E-8 W/(m²-K⁴) (4.76E-13 Btu/(s-ft²-R⁴))
α_s = absorptivity of exposed boundary surface, dimensionless
ϵ_s = emissivity of exposed boundary surface, dimensionless
ϵ_f = emissivity of exposing fire surface, dimensionless
T_f = known or given fire temperature K (R)

Equivalently,

$$\dot{q}''_{rad} = h_r(T_\infty - T_s) \quad (5)$$

or

$$h_r \approx \dot{q}''_{rad}/(T_f - T_o) \quad \text{(most conservative)}$$

where

h_r = radiative heat transfer coefficient W/(m²-K) (Btu/(s-ft²-R))
T_f = assumed fire temperature 1366.7K (2000°F)
T_o = initial ambient temperature 294.4 K (70°F)

For simplicity, h_r and $\dot{q}''_{rad}$ are functions of T_f and T_o only, which both are constant in the current discussion. This simplification yields the most conservative results. If the view factor and all radiative properties are unity, then h_r is approximated 184.1 W/(m²-K) (9.0E-3 Btu/(s-ft²-R)).

Clearly, as the time marches on, the *a priori* unknown *net* (versus incident) flux strongly dependent of $(T_f - T_s)$ would rapidly decrease as the exposed surface temperatures asymptotically approach but never attain the fire temperature. Therefore, caution is needed when substituting a constant or time-varying prescribed flux boundary condition (or *a priori* known *constant incident* heat flux usually based on empirical or experimental data) for the *net* flux. Eventually, the prescribed flux would lead to a nonphysical phenomenon; i.e., the surface temperature will be greater than the fire temperature. A prime example of this pitfall is to unconditionally feed a substantially constant "incident" heat flux (versus *net* heat flux for convective boundaries) into the analytical Semi-Infinite Slab Model for a prolonged exposure.

NONDIMENSIONALIZATION

To consider nonlinear, time- or temperature-dependent boundary conditions or thermophysical properties, we are forced to use numerical or computerized solutions, since there would be no easily available analytical solutions. Nondimensionalization analysis of governing equations (e.g., Eqs (1)–(5)) is prevalent in the community of computational science. Although nondimensionalization is only a recommended practice and

not necessary for any numerical algorithm, the practice offers some salient numerical advantages. Foremost, it reveals the magnitudes of dimensionless transport groups resulting from the user-selected time and length scales, which, in some cases, crucially dictate the successes of numerical implementations. Secondly, ranges of discretized temporal and spatial domains, numerical solutions (dependent variables), and certain transport properties, usually are normalized between 0 and 1, thereby facilitating the numerical analysis and minimizing potential numerical difficulties.

Arbitrarily defining the following dimensionless parameters,

$$x^* \equiv \frac{x}{L} \qquad t^* \equiv \frac{t}{t_o}$$

$$T^* \equiv \frac{T_{max} - T}{T_{max} - T_{min}} = \frac{T_{max} - T}{\Delta T_o}$$

$$k^* \equiv \frac{k}{k_o} \qquad Fo \equiv \frac{\alpha t_o}{L^2} \tag{6}$$

$$\dot{q}''_{cond,o} = \frac{\Delta T_o k_o}{L}$$

$$\dot{q}''_{conv,o} = \Delta T_o h_o = \Delta T_o (h_c + h_r)$$

$$\dot{q}'''_o = \frac{\dot{q}''_{cond,o}}{L} \qquad \dot{q}''' = \frac{\dot{q}'''^*}{\dot{q}'''_o}$$

where

α = thermal diffusivity = $\frac{k}{\rho c_p}$ m²/s (ft²/s)

Fo = Fourier number

Eqs (1)–(6), in the absence of internal heat generation, become

$$\frac{\partial}{\partial x^*}\left(k^* \frac{\partial T^*}{\partial x^*}\right) + \frac{\partial}{\partial y^*}\left(k^* \frac{\partial T^*}{\partial y^*}\right) + \frac{\partial}{\partial z^*}\left(k^* \frac{\partial T^*}{\partial z^*}\right) = \frac{1}{Fo} \frac{\partial T^*}{\partial t^*} \tag{7}$$

with the following generic scalar boundary conditions

$$-k^* \frac{\partial T^*}{\partial n} = h^* Bi (T^*_\infty - T^*_s) \tag{8}$$

where

$h^* = h/h_o$

$h_o = h_c + h_r = (25.0 + 184.1) = 209.1$ kW/(m²-K) (1.02E-2 Btu/(s-ft²-R))

Bi = Biot (Nusselt) number = $\frac{\dot{q}''_{o,conv}}{\dot{q}''_{o,cond}} = \frac{(\Delta T_o) h_o}{(\Delta T_o) k_o / L} = \frac{h_o L}{k_o}$

$T^*_\infty = T^*_f$ or T^*_o

or

$T^*_s = T^*_f$ or T^*_o
(prescribed (Dirichlet) boundary condition) (9)

For simplicity, if $h = h_o$ then h^* equals unity and hence disappears in Eq (8).

The initial condition is

$$T^*(x^*, y^*, z^*, t^* = 0) = T^*_o \tag{10}$$

One exception for Eq (10) is a prescribed constant or time-dependent temperature boundary; e.g., $T^*(x^* = 0 \text{ or } 1, y^*, z^*, t^* = 0) = T^*_f$.

Numerical Algorithm

The most simple numerical solution procedure for Eqs (6)–(9) is the Explicit Finite Difference Scheme based on Taylor Series, which in its final form, is merely a trivial algebraic expression that can be easily understood and implemented by an average fire professional or engineer. For simplicity, constant thermophysical properties and uniform discretizations of dimensionless time step and spatial domain are assumed.

One-Dimensional

In Figure 1, the dimensionless physical domain ($0 \le x^* \le 1$) is discretized by M equal lengths (cell or control volume) denoted by Δx^*s which are joined by (M + 1) nodal points. Each node is desig-

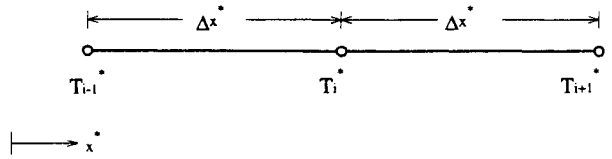

Figure 1. 1-D Interior Domain

nated a dimensionless discretized temperature at the x^* location. For example, a generic set of three nodal locations of the interior domain. Nodes i, i − 1 and i + 1 denote any arbitrarily interior node, its backward and forward nodes, respectively. At any given $t^* = n\Delta t^*$, where n is the number of dimensionless discretized time steps Δt^*, the incremental dimensionless temperature of a generic Node i of the interior spatial domain is

$$\Delta T_i^* = d(T_{i-1}^* + T_{i+1}^* - 2T_i^*)_n \qquad (11)$$

where

$$d \equiv Fo\frac{\alpha^*\Delta t^*}{(\Delta x^*)^2} = \text{dimensionless diffusion number}$$

$$\alpha^* \equiv \frac{\alpha}{\alpha_o} = \text{dimensionless diffusivity}$$

For constant thermophysical properties, $\alpha = \alpha_o$ and $\alpha^* = 1.0$.

Hence, the new temperature of T_i^* at Node i for the next time interval, n + 1, is

$$(T_i^*)_{n+1} = (T_i^*)_n + \Delta T_i^* \qquad (12)$$

Subscript n denotes the *current* time interval at which values of T_i^*, T_{i-1}^* and T_{i+1}^* for Nodes i, i − 1 and i + 1, respectively, are *a priori* or explicitly known. The procedure begins with the initial condition when every discretized nodal temperature is at the same initial temperature (normally at room temperature 294.4 K (70°F)) except for prescribed nodal surface temperatures. Subsequently, all interior temperatures can be determined by Eqs (11) and (12).

In Figure 2, a typical convective boundary is shown at $x^* = 0$. The conservation law of energy rate in conjunction with a three-point forward (or backward) finite-difference scheme is invoked at this boundary node,

$$\Delta T_s^* = 2d\{H(T_\infty^* - T_s^*) + (T_{i+1}^* + T_{i+2}^* - 2T_s^*)/3\}_n \qquad \text{(1st-order accuracy)} \quad (13)$$

or

$$\Delta T_s^* = 2d\{H(T_\infty^* - T_s^*) + (4T_{i+1}^* - T_{i+2}^* - 3T_s^*)/2\}_n \qquad \text{(2nd-order accuracy)}$$

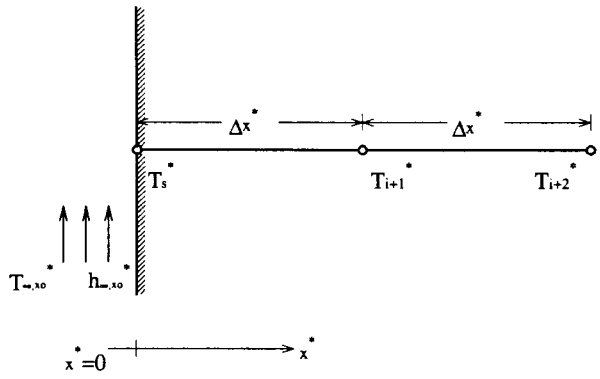

Figure 2. 1-D Boundary

where

$$H \equiv \frac{Bi(\Delta x^*)h^*}{k^*}$$

Again, for constant thermophysical properties, $k = k_o$ and hence $k^* = 1.0$. Depending on the user's basic assumptions of the fire specifications, h^* can be unity or variable (time-dependent). For uniform temporal and spatial meshes, both d and H are dimensionless constants, provided that the thermophysical properties of the assembly and overall heat transfer coefficient from the fire are constant. Subscript s denotes either the exposed surface (boundary) node at $x^* = 0$ or the unexposed surface at $x^* = 1$. For $x^* = 1$, Eq (13) still applies, by replacing Subscripts i + 1 and i + 2 with i − 1 and i − 2, respectively.

For prescribed *constant* temperature boundary nodes (boundary condition of first kind), $\Delta T_s^* = 0$. If however a variable or time-dependent temperature is prescribed at the exposed (surface) node, $T_s^* = T_s^*(x^*,t^*)$. A prime example of this type of boundary condition would be the famous ASTM E119 or ISO 834 Time-Temperature Fire Curve. Two- and three-dimensional schemes are merely the natural extensions of the above one-dimensional scheme. Overall, Eq (13) is in the first-order accuracy, since Δt is invariantly first-order accuracy due to the nature of explicit scheme, despite the available choice of second-order or higher-order accuracy for any spatial coordinate. Although the selection of the boundary condition of second kind is deemed inappropriate or rarely justified, its expressions for this one-dimensional case (for reference only) are as follows,

$$\Delta T_s^* = 2d\{H_N\dot{q}''^* + (T_{i+1}^* + T_{i+2}^* - 2T_s^*)/3\}_n \qquad (14)$$

where

$$H_N \equiv \frac{\Delta x^*}{k^*}$$

$$\dot{q}_o'' = \frac{\Delta T_o k_o}{L} \text{ (arbitrary but based on Fourier Law)}$$

W/m^2 (Btu/(s-ft^2))

If the adiabatic boundary is justified, the unexposed surface temperature is,

$$\Delta T_s^* = 2d\{(T_{i-1}^* + T_{i-2}^* - 2T_s^*)/3\}_n \quad (15)$$

Two-Dimensional

By extending j index in the y-direction and setting $\Delta x^* = \Delta y^*$ (uniform mesh) in Figure 3, the incremental nodal temperature at the intersection of ith-row and jth-column in a dimensionless uniform two-dimensional mesh is

$$\Delta T_{ij}^* = d(T_{i-1}^* + T_{i+1}^* + T_{j-1}^* + T_{j+1}^* - 4T_{ij}^*)_n \quad (16)$$

The same diffusion number d applies. For clarity, only single subscript is used, except for the interested node, which has a dual subscript. To determine the new temperature at Node ij at the next time interval, Eq (12) still applies. For a Cartesian coordinate system, there are four corner nodes and four sets of edge nodes. For a "southwest" corner node,

$$\Delta T_s^* = 2d\{[H_{\infty,x}(T_{\infty,x}^* - T_s^*) + H_{\infty,y}(T_{\infty,y}^* - T_s^*)] + (T_{i+1}^* + T_{i+2}^* + T_{j+1}^* + T_{j+2}^* - 4T_s^*)/3\}_n \quad (17)$$

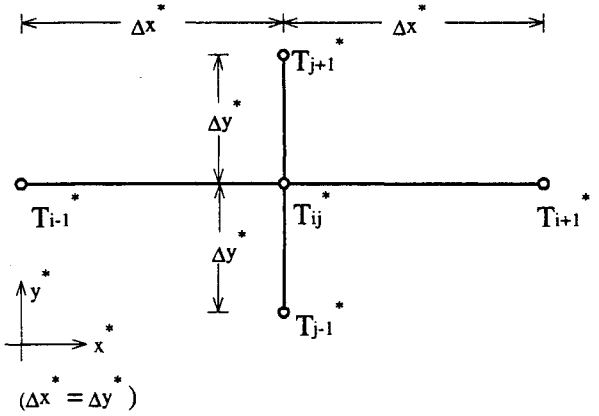

Figure 3. 2-D Interior Domain

Preserving the same definition in Eq (13), H here is the conglomerate dimensionless overall heat transfer coefficient from the fire. Subscripts ∞,x and ∞,y in H and T* identify the sides (boundaries) of the spatial domain. For example, in Eq (17), subscript ∞,x denotes the west boundary or $x^* = 0$. The other three corner nodes can be easily inferred by reversing the signs of i or j indices (subscripts). Likewise, the incremental temperature of a generic west boundary node at $x^* = 0$ is

$$\Delta T_s^* = 2d\{H_{\infty,x}(T_{\infty,x}^* - T_s^*) + (2T_{i+1}^* + 2T_{i+2}^* + 3T_{j-1}^* + 3T_{j+1}^* - 10T_s^*)/6\} \quad (18)$$

The 3-point central-difference method is applied to the y-temperature gradient, whereas the 3-point forward finite-difference method remains in the x-direction. And a generic boundary node at the south edge or $y^* = 0$ is

$$\Delta T_s^* = 2d\{H_{\infty,y}(T_{\infty,y}^* - T_s^*) + (3T_{i-1}^* + 3T_{i+1}^* + 2T_{j+1}^* + 2T_{j+2}^* - 10T_s^*)/6\}_n \quad (19)$$

By manipulating the signs of the indices typically shown in Figure 4, discretization equations for east and north boundary nodes can be easily derived.

Three-Dimensional

By adding a third index k in the z-direction in Figure 5, the incremental temperature of a generic interior node is

$$\Delta T_{ijk}^* = d(T_{i-1}^* + T_{i+1}^* + T_{j-1}^* + T_{j+1}^* + T_{k-1}^* + T_{k+1}^* - 6T_{ijk}^*)_n \quad (20)$$

A generic corner node at the origin of the Cartesian coordinate system is

$$\Delta T_s^* = 2d\{[H_{\infty,x}(T_{\infty,x}^* - T_s^*) + H_{\infty,y}(T_{\infty,y}^* - T_s^*) + H_{\infty,z}(T_{\infty,z}^* - T_s^*)] + (T_{i+1}^* + T_{i+2}^* + T_{j+1}^* + T_{j+2}^* + T_{k+1}^* + T_{k+2}^* - 6T_s^*)/3\}_n \quad (21)$$

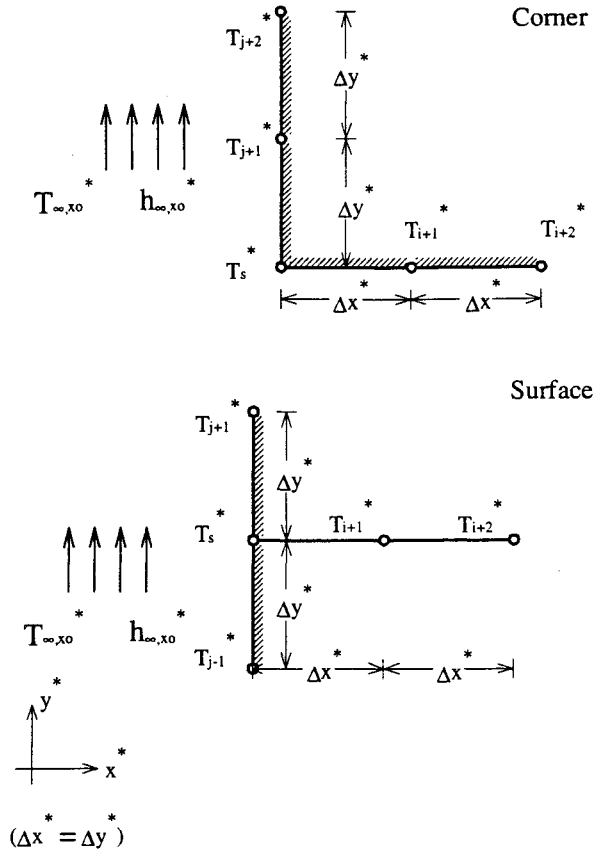

Figure 4. 2-D Boundary

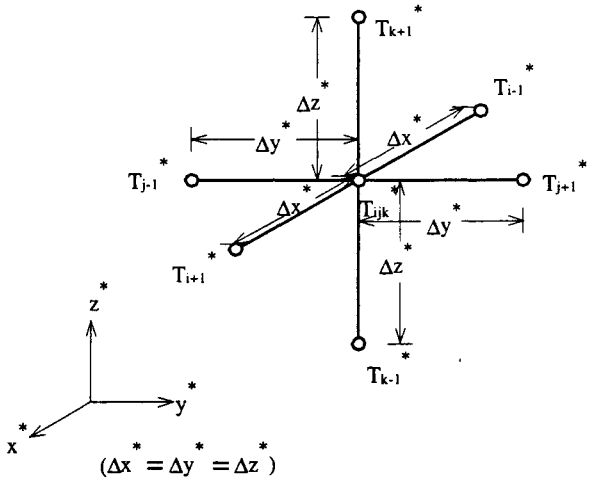

Figure 5. 3-D Interior Domain

A generic edge node along y*-axis is

$$\Delta T_s^* = 2d\{[H_{\infty,x}(T_{\infty,x}^* - T_s^*) + H_{\infty,z}(T_{\infty,z}^* - T_s^*)] + (2T_{i+1}^* + 2T_{i+2}^* + 3T_{j-1}^* + 3T_{j+1}^* + 2T_{k+1}^* + 2T_{k+2}^* - 14T_s^*)/6\}_n \quad (22)$$

A generic surface node on $z^* = 0$ plane is

$$\Delta T_s^* = 2d\{H_{\infty,z}(T_{\infty,z}^* - T_s^*) + (3T_{i-1}^* + 3T_{i+1}^* + 3T_{j-1}^* + 3T_{j+1}^* + 2T_{k+1}^* + 2K_{k+2}^* - 16T_s^*)/6\}_n \quad (23)$$

Again, all other corners, edges and surfaces, typically shown in Figure 6, share the same generic formulas but different or reverse indices.

NUMERICAL EXAMPLES

Let L = 0.3 m (11.8 in) and the test material be generic concrete[4]: k = 1.4 W/(m-K) (2.25E-4 Btu/(s-ft-R)), $\rho = 2300$ kg/m^3 (143.58 lb$_m$/ft^3), c_p = 880 J/(kg-K) (0.21 Btu/(lb$_m$-R)) and

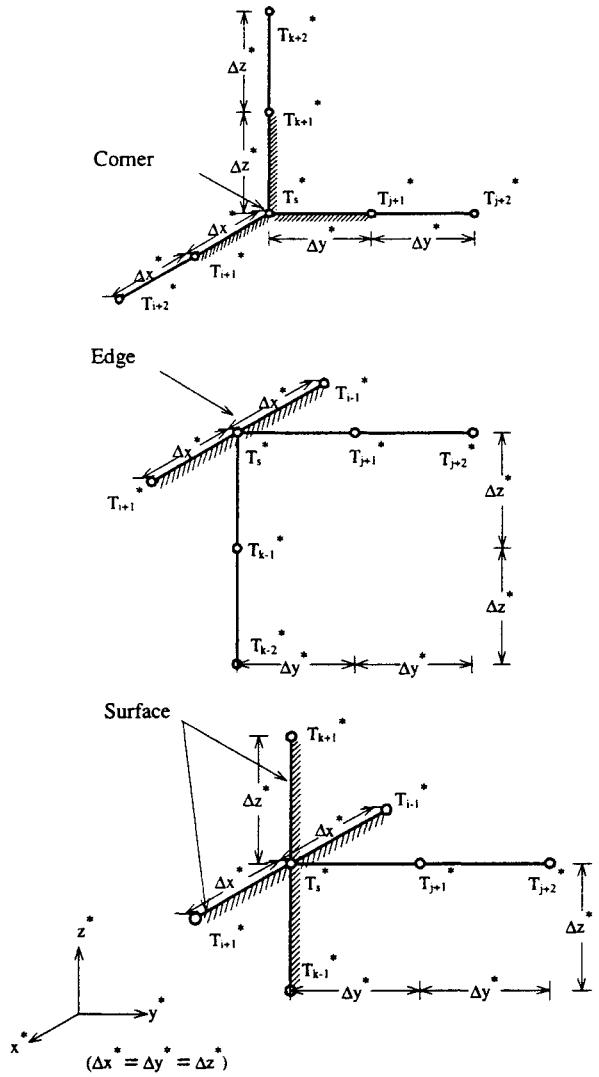

Figure 6. 3-D Boundary

$\alpha = 6.917E\text{-}7$ m²/s (7.445E-6 ft²/s). Further, the fire specifications are: $T_f = 1366.7$ K (2000°F), $T_o = 294.4$ K (70°F), $h_o = 209.1$ W/(m²-K) (1.02E-2 Btu/(s-ft²-R)). The arbitrarily selected reference time t_o is 3600 s; thus, Fo = 0.027668, Bi = 44.8, and the simulation period is 3 hours. The numerical results are divided between constant surface (Dirichlet) temperature and convective (Robin) boundary conditions. Each group is subdivided into three different dimensionalities. The fire boundary conditions are at $x^* = 0$ and 1; $y^* = 0$ and 1; and $z^* = 0$ and 1. The same fire exposure is applied to every corner, edge and surface of the one-, two-, and three-dimensional domains. The numerical experiment for both groups consists of four different meshes and three different time steps.

Prior to graphically presenting the "final" numerical results, it is crucial that a cogent process of numerical stability and accuracy be performed. To facilitate this study, representing nodal temperatures at the following locations are selected: exposed surface ($x^* = 0$); 1/4 slab thickness ($x^* = 1/4$); and mid-plane slab thickness ($x^* = 1/2$). Tables 1–3 summarize the numerical stability and convergence studies for these nodal temperatures after 3-hour fire exposure, which is based on prescribed constant fire temperature at exposed surfaces; i.e., $T_s = T_f$. Interior temperatures $T_{1/4}$ and $T_{1/2}$ denote the nodal temperatures at ¼ and ½ of the slab thickness (length), respectively. For two-dimensional meshes, these nodal temperatures are along the symmetrical line $x^* = 0.5$ or $y^* = 0.5$; for three-dimensional meshes, these nodes are located inside *one* of the three mutually perpendicular planes of which centers coincide with the symmetrical center of the 3-D physical domain; i.e., $x^* = y^* = z^* = 0.5$. For clarity, conversions to Fahrenheit temperature are omitted.

Tables 4–6 summarize numerical results under convective (Robin) or time-varying heat flux boundaries.

The major concerns of any numerical procedure, even for the simple one here, are numerical stability (robustness) and accuracy, which are the cruxes of computational science. Numerical efficiency dealing with minimization of utilization of time steps (hence cpu time) or memory, or both, is also an important but a secondary issue. Discussions of Von Neumann Stability [e.g., Refs. 5–7] and Linear Elliptic, Parabolic and Hyperbolic Partial Differential Equations Convergence and Error Analysis [e.g., Ref. 8] and other related advanced theories which are the theoretical bases for the error study, are beyond the scope of this paper. In a nutshell, any *arbitrary* set of temporal and spatial disretizations may not be appropriate or adequately dense for a particular engineering problem. The diffusion number $\Sigma d_j \leq$ ½ (j = 1, 2, or 3 dimensions) usually provides useful hints concerning *stability only*. However, as a "safe" guideline, though time-consuming, we always parameterize both Δx^* and Δt^* to see if a "convincing" pattern of numerical solutions *converging* to *the* uniquely

Table 1. 1-D Prescribed Constant Exposed Surface Temperature

Δt, s	M	d	T_s, K	$T_{1/4}$, K	$T_{1/2}$, K
100	10	0.8540	1366.7	948.1	768.1
100	20	3.4158	1366.7	942.5	767.3
100	40	13.66	div	div	div
100	80	54.65	div	div	div
10	10	0.0854	1366.7	946.9	766.5
10	20	0.34158	1366.7	941.2	765.6
10	40	1.366	1366.7	941.1	765.4
10	80	5.465	1366.7	941.1	765.4
1	10	0.00854	1366.7	946.8	766.3
1	20	0.034158	1366.7	941.1	765.5
1	40	0.1366	1366.7	941.0	765.3
1	80	0.5465	1366.7	941.0	765.2

div = divergent solution

Table 2. 2-D Prescribed Constant Exposed Surface Temperature

Δt, s	M	d	T_s, K	$T_{1/4}$, K	$T_{1/2}$, K
100	10×10	0.8540	1366.7	1138.0	1039.5
100	20×20	3.4158	div	div	div
100	40×40	13.66	div	div	div
100	80×80	54.65	div	div	div
10	10×10	0.0854	1366.7	1131.9	1030.9
10	20×20	0.34158	1366.7	1128.4	1030.0
10	40×40	1.366	1366.7	1128.2	1029.8
10	80×80	5.465	div	div	div
1	10×10	0.00854	1366.7	1131.7	1030.6
1	20×20	0.034158	1366.7	1128.2	1029.7
1	40×40	0.1366	1366.7	1128.0	1029.5
1	80×80	0.5465	1366.7	1128.0	1029.4

Table 3. 3-D Prescribed Constant Exposed Surface Temperature

Δt, s	M	d	T_s, K	$T_{1/4}$, K	$T_{1/2}$, K
100	10×10×10	0.8540	1366.7	1241.5	1187.7
100	20×20×20	3.4158	div	div	div
100	40×40×40	13.66	div	div	div
100	80×80×80	54.65	div	div	div
10	10×10×10	0.0854	1366.7	1235.7	1179.4
10	20×20×20	0.34158	1366.7	1233.6	1178.6
10	40×40×40	1.366	1366.7	1233.5	1178.4
10	80×80×80	5.465	div	div	div
1	10×10×10	0.00854	1366.7	1235.1	1178.6
1	20×20×20	0.034158	1366.7	1233.0	1177.8
1	40×40×40	0.1366	1366.7	1232.8	1177.6
1	80×80×80	0.5465	1366.7	1232.8	1177.5

Table 4. 1-D Convective Exposed Surface Flux

Δt, s	M	d	T_s, K	$T_{1/4}$, K	$T_{1/2}$, K
100	10	0.8540	1326.1	907.3	730.4
100	20	3.4158	1324.4	899.8	728.0
100	40	13.66	div	div	div
100	80	54.65	div	div	div
10	10	0.0854	1325.9	906.1	729.0
10	20	0.34158	1324.3	898.6	726.5
10	40	1.366	1323.8	897.7	725.4
10	80	5.465	1323.6	897.2	724.9
1	10	0.00854	1325.9	906.0	728.9
1	20	0.034158	1324.3	898.5	726.4
1	40	0.1366	1323.8	897.6	725.3
1	80	0.5465	1323.6	897.1	724.7

Table 5. 2-D Convective Exposed Surface Flux

Δt, s	M	d	T_s, K	$T_{1/4}$, K	$T_{1/2}$, K
100	10×10	0.8540	1343.0	1099.3	996.3
100	20×20	3.4158	div	div	div
100	40×40	13.66	div	div	div
100	80×80	54.65	div	div	div
10	10×10	0.0854	1342.5	1093.0	987.7
10	20×20	0.34158	1341.4	1087.4	984.7
10	40×40	1.366	1341.1	1086.3	983.4
10	80×80	5.465	div	div	div
1	10×10	0.00854	1342.5	1092.7	987.4
1	20×20	0.034158	1341.4	1087.2	984.4
1	40×40	0.1366	1341.0	1086.1	983.1
1	80×80	0.5465	1340.9	1085.6	982.4

Table 6. 3-D Convective Exposed Surface Flux

Δt, s	M	d	T_s, K	$T_{1/4}$, K	$T_{1/2}$, K
100	10×10×10	0.8540	div	div	div
100	20×20×20	3.4158	div	div	div
100	40×40×40	13.66	div	div	div
100	80×80×80	54.65	div	div	div
10	10×10×10	0.0854	1352.3	1204.4	1142.0
10	20×20×20	0.34158	1351.6	1200.5	1139.4
10	40×40×40	1.366	1351.3	1198.6	1135.0
10	80×80×80	5.465	div	div	div
1	10×10×10	0.00854	1353.3	1203.8	1141.1
1	20×20×20	0.034158	1351.6	1199.8	1138.5
1	40×40×40	0.1366	1351.2	1197.2	1137.2
1	80×80×80	0.5465	1351.1	1197.1	1134.9

"true" solution has been established. In this sense, the numerical approach is more an art than a science. Unaware of the numerical accuracy or difficulties in general, some fire professionals are easily tempted by the *stable* numerical solutions without further investigating the solution accuracy. Converged *and* unique solutions are truly independent of *any* "randomly" selected set of temporal and spatial discretizations, which must be numerically consistent, stable and convergent.

Without any rigorous error analysis, we are convinced that by inspection, the temporal-spatial discretization: $\Delta x^* = 0.05$ ($\Delta x = 0.015$ m) or M = 20 elements, and $\Delta t^* = 2.7778\text{E-}3$ ($\Delta t = 10$ s), has converged to the "true" solution with acceptable bounded errors. Thus, the above six simulations, i.e., Tables 1–6, are summarized in Figure 7. The coolest temperature profile is one-dimensional convective exposed surface; and the hottest temperature profile is three-dimensional constant-temperature exposed surface. The temperature difference at the mid-plane between these two cases is (1178.6-726.5) K = 452.1 K, whereas the temperature variations among all cases at the exposed surface are relatively minimal; i.e., 1320~1367 K.

Numerical Performance

A general methodology for securing a quality, *converging* numerical solution has been dis-

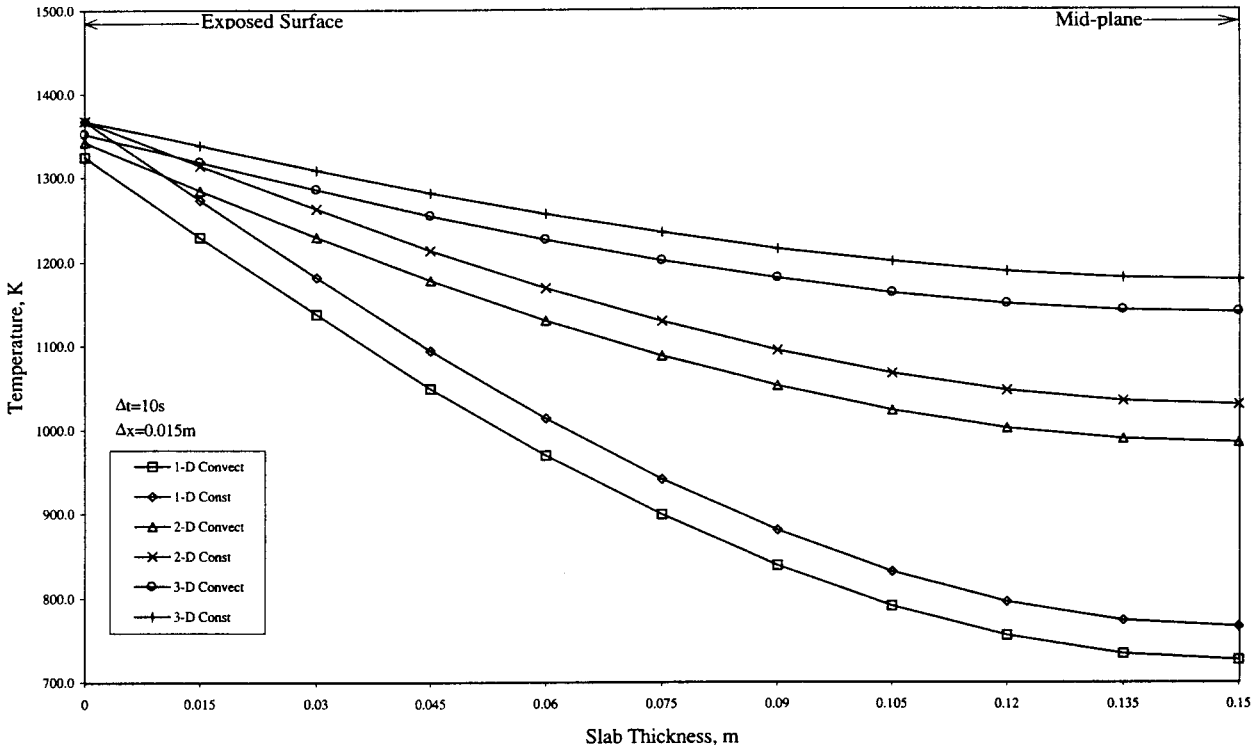

Figure 7. Sumary of Constant Properties Results

cussed. But how *good* is this so-called converging solution? Or, how good is this "user-friendly" algorithm, from the purely mathematical standpoint? This question falls under one of the common issues belonging to numerical performance. Foremost, we need a benchmark case; and in this special example, analytical solutions are available for comparison. Table 7 summarizes the analytical solutions.

Comparing Tables 1–6 with Table 7, one can conclude that the constant temperature (Dirichlet) boundaries perform very well, whereas numerical results of the convective flux (Robin) boundaries are "reasonable" and may need some improvements, depending on the expected or user-defined error bounds of the numerical solutions. Other more complicated or advanced algorithms such as higher-order Explicit and Implicit Finite Difference, Finite Volume and Finite Element *may* improve the accuracy. Furthermore, non-uniform meshes packing more nodes near the boundaries may be helpful. Unfortunately, incorporation of any or some of these algorithms would substantially revise the simple or "user-friendly" algorithm introduced here. Readers should be cautioned that any or even the "best" numerical algorithm only provides *approximated*

Table 7. Analytical Solutions

	T_s, K	$T_{1/4}$, K	$T_{1/2}$, K
Constant Temp.			
1-D	1366.7	941.0	765.2
2-D	1366.7	1127.9	1029.3
3-D	1366.7	1232.7	1177.4
Convective Flux			
1-D	1324.6	913.4	768.1
2-D	1308.9	928.5	869.8
3-D	1327.3	1068.4	1028.4

solutions, intrinsically possessing some numerical errors *permanently* deviating from the unique, true solutions for certain classes of engineering problems.

NONLINEAR PROBLEMS

The usefulness of any numerical procedure is rather minimal if it is limited to linear problems for which analytical solutions are often available. However, to assess the performance of the algorithm and to verify its concomitant software, a simple benchmark case restricted to linear problems is usually necessary. Once this crucial step has been verified, the algorithm can be easily expanded to nonlinear problems. Without the loss of generality of Eqs (11)–(23), incorporation of variable (temperature-dependent) thermophysical properties, or variable (temporal) fire temperature, or both, is fairly simple.

One-Dimensional Nonlinear

With a minimal modification, Eq (11) can be easily revised to accommodate the variable or temperature-dependent thermal conductivity of the concrete assembly,

$$\Delta T_i^* = d_V(k_{i-1}^* T_{i-1}^* + k_{k+1}^* T_{i+1}^* - 2k_i^* T_i^*)_n \qquad (24)$$

where

$$d_V \equiv Fo\left(\frac{\Delta t^*}{\rho_i^* c_{p,i}^* (\Delta x^*)^2}\right)$$

$= \textit{variable}$ dimensionless diffusion number

Similar to Eq (13), the incremental boundary temperature is

$$\Delta T_s^* = 2d_V\{H_V(T_\infty^* - T_s^*) + (k_{i-1}^* T_{i-1}^* + k_{i+1}^* T_{i+1}^* - 2k_i^* T_i^*)/3\}_n \qquad (25)$$

where

$$H_V = Bi(\Delta x^*)h^*$$

Since Biot number Bi is a fixed number and Δx^* is constant (as a result of uniform mesh), H_v can be either constant or variable depending on whether h* equals unity. Although the incorporation of variable conductivity is straightforward, the resultant impact of computer programming may be profound. The diffusion number here is no longer a constant because ρ^* and c_p^* are functions of temperature which in turn are functions of time. For example, before the algorithm modification, the programming for Eqs (11) and (12) is virtually effortless, since the entire computer code consists of a few "user-friendly" or trivial lines. Now, linear interpolations for all thermophysical properties are required at each node *and* each time station, thereby significantly complicating the programming and imposing more stringent hardware requirements in terms of memory and cpu speed.

Two-Dimensional Nonlinear

Using the same indicial designations as before, the incremental temperature of a generic interior node is

$$\Delta T_{ij}^* = d_V(k_{i-1}^* T_{i-1}^* + k_{i+1}^* T_{i+1}^* + k_{j-1}^* T_{j-1}^* + k_{j+1}^* T_{j+1}^* - 4k_{ij}^* T_{ij}^*)_n \qquad (26)$$

For a southwest corner node,

$$\Delta T_s^* = 2d_V\{[H_{V\infty,x}(T_{\infty,x}^* - T_s^*) + H_{V\infty,y}(T_{\infty,y}^* - T_s^*)] + (k_{i+1}^* T_{i+1}^* + k_{i+2}^* T_{i+2}^* + k_{j+1}^* T_{j+1}^* + k_{i+2}^* T_{j+2}^* - 4k_{ij}^* T_s^*)/3\}_n \qquad (27)$$

The incremental temperature of a generic west boundary node at $x^* = 0$ is

$$\Delta T_s^* = 2d_V\{H_{V\infty,x}(T_{\infty,x}^* - T_s^*) + (2k_{i+1}^* T_{i+1}^* + 2k_{i+2}^* T_{i+2}^* + 3k_{j-1}^* T_{j-1}^* + 3k_{j+1}^* T_{j+1}^* - 10k_{ij}^* T_s^*)/6\} \qquad (28)$$

And a generic boundary node at the south edge or $y^* = 0$ is

$$\Delta T_s^* = 2d_V\{H_{V\infty,y}(T_{\infty,y}^* - T_s^*) + (3k_{i-1}^* T_{i-1}^* + 3k_{i+1}^* T_{i+1}^* + 2k_{j+1}^* T_{j+1}^* + 2k_{j+2}^* T_{j+2}^* - 10k_{ij}^* T_s^*)/6\}_n \qquad (29)$$

Three-Dimensional Nonlinear

A generic interior node is

$$\begin{aligned}\Delta T^*_{ijk} = d_V(&k^*_{i-1}T^*_{i-1}+k^*_{i+1}T^*_{i+1}\\&+k^*_{j-1}T^*_{j-1}+k^*_{j+1}T^*_{j+1}+k^*_{k-1}T^*_{k-1}\\&+k^*_{k+1}T^*_{k+1}-6k^*_{ijk}T^*_{ijk})_n\end{aligned} \quad (30)$$

The variable diffusion number is the same as the diffusion number defined in Eq (24), where $\Delta x^* = \Delta y^* = \Delta z^*$ for uniform meshes. A generic corner node, e.g., at the origin of the three-dimensional Cartesian coordinate system, is

$$\begin{aligned}\Delta T^*_s = 2d_V\{&[H_{V\infty,x}(T^*_{\infty,x}-T^*_s)+H_{V\infty,y}(T^*_{\infty,y}-T^*_s)\\&+H_{V\infty,z}(T^*_{\infty,z}-T^*_s)]+(k^*_{i+1}T^*_{i+1}+k^*_{i+2}T^*_{i+2}\\&+k^*_{j+1}T^*_{j+1}+k^*_{j+2}T^*_{j+2}+k^*_{k+1}T^*_{k+1}\\&+k^*_{k+2}T^*_{k+2}-6\,k^*_{ijk}T^*_s)/3\}_n\end{aligned} \quad (31)$$

A generic edge node along y*-axis is

$$\begin{aligned}\Delta T^*_s = 2d_V\{&[H_{V\infty,x}(T^*_{\infty,x}-T^*_s)+H_{V\infty,z}(T^*_{\infty,z}-T^*_s)]\\&+(2k^*_{i+1}T^*_{i+1}+2k^*_{i+2}T^*_{i+2}+2k^*_{j-1}T^*_{j-1}\\&+2\,k^*_{j+1}T^*_{j+1}+3k^*_{k+1}T^*_{k+1}\\&+3k^*_{k+2}T^*_{k+2}-14k^*_{ijj}T^*_s)/6\}_n\end{aligned} \quad (32)$$

A generic surface node at $z^* = 0$ plane is

$$\begin{aligned}\Delta T^*_s = 2d_V\{&H_{V\infty,z}(T^*_{\infty,z}-T^*_s)\\&+(3k^*_{i-1}T^*_{i-1}+3k^*_{i+1}T^*_{i+1}+3k^*_{j-1}T^*_{j-1}\\&+3k^*_{j+1}T^*_{j+1}+2k^*_{k+1}T^*_{k+1}\\&+2\,k^*_{k+2}T^*_{k+2}-16T^*_s)/6\}_n\end{aligned} \quad (33)$$

As an example, the same problem definition formulated in the previous linear model is repeated here. Same constant density and specific heat of generic concrete are assumed. Consequently, the only nonlinearity arising from this nonlinear model is the variable (temperature-dependent) thermal conductivity, which is extracted from Gross' experimental data for generic normal weight concrete as shown in Table 8.[9]

Upon completion of a careful study of numerical stability and convergence, numerical results from the spatial-temporal discretization of $M = 20$, $\Delta x = 0.015$ m, and $\Delta t = 10$ s, are acceptable and hence plotted in Figure 8. Qualitatively, the temperature profiles between the linear and nonlinear models are similar except for the "steep" concavities near the exposed surface for the nonlinear model. Overall, the nonlinear temperature profiles are moderately lower due to lower thermal conductivities at elevated temperatures (Table 8).

Time-Dependent Fire Source and Internal Heat Generation Rate

With respect to a temporal fire, simply $T^*_f = T^*_f(t^*)$. Discrete fire temperature can be read at each time interval. If desired, $h = h(T_f(t), T_s(t))$. Additional refinements for predominantly temporal-radiative effects in Eqs (4) and (5) can also be considered. For fire damageability studies in terms of ignition temperature and critical heat flux, the engineering model considered herein can predict the temporal exposed surface temperature or *net* flux, or both. However, an additional formulation and expensive computations are needed for the complex view factor from the differential target area to the three-dimensional exposing fire surface area. This view factor for all intents and purposes is much less than unity, since, unlike the furnace situation, the interested target (e.g., sprinkler, heat detector, equipment, and human skin) usually is located several meters (or more) away from the flame.

If a heat source or sink exists at an interior node, Eq (24) becomes

$$\begin{aligned}\Delta T^*_i = d(&k^*_{i-1}T^*_{i-1}+k^*_{i+1}T^*_{i+1}\\&-2k^*_iT^*_i+\dot{q}'''_i(\Delta x^*)^2)_n\end{aligned} \quad (34)$$

A Practical Example

Although it is imperative to verify numerical solution integrity, it is equally or more important to find out how good the engineering model (i.e., Eq (1)) is. As a simple example, the one-dimensional linear and nonlinear models are applied to simulate an ASTM E119 or ISO 834 fire test for a solid homogeneous concrete slab of 1.575 m (6.2 in) thickness. Generically, appearing in many literature [e.g., Ref. 10], and US building

Table 8. Variable Thermal Conductivity of Normal Weight Concrete

Temp, K	≤293.0	373.0	473.0	773.0	≥1073.0
k, W/(m-K)	1.75	1.7	1.38	0.9	0.6

codes, this thickness can endure a 3-hour fire test. This implies that the unexposed surface temperature normally would not exceed 433 K (320°F) at the end of the test, e.g., Ref. [11].

For simplicity, the temporal fire temperature $T_f(t)$ or temporal overall convective heat transfer coefficient h(t) is not adopted. Instead, a constant h (hence T_f) is used. Again, the previous constant thermophysical properties are assumed, with the exception of the variable thermal conductivity (Table 8) for the nonlinear model. To test the sensitive variation of h (or T_f), one-half of h (i.e., $h = 104.6$ W/(m^2-K)) is used in addition to $h = 209.1$ W/(m^2-K). This practical simulation consists of four runs: (1) constant properties (linear) and $h = 209.1$ W/(m^2-K); (2) constant properties (linear) and $h = 104.6$ W/(m^2-K); (3) variable properties (nonlinear) and $h = 209.1$ W/(m^2-K); and (4) variable properties (nonlinear) and $h = 104.6$ W/(m^2-K). The assumed ambient air temperature and overall convective heat transfer coefficient at the unexposed surface are 294.4 K and 25 W/(m^2-K), respectively. The verified sets of spatial-temporal temperature profiles for all of these linear and nonlinear runs, based on $M = 20$ or $\Delta x = 0.007875$ m and $\Delta t = 10$ s, are plotted in Figure 9.

The first observation is that the same nonlinear "concavities" display in Figure 9, qualitatively signifying the major difference of temperature profiles between the linear and nonlinear models. The second observation is that despite concavities signifying lower temperatures, at the unexposed surface, nonlinear temperatures are slightly *greater* than the linear temperatures. The third observation is that neither model is sensitive to the exposed convective heat transfer coefficient, based on this limited range of coefficient.

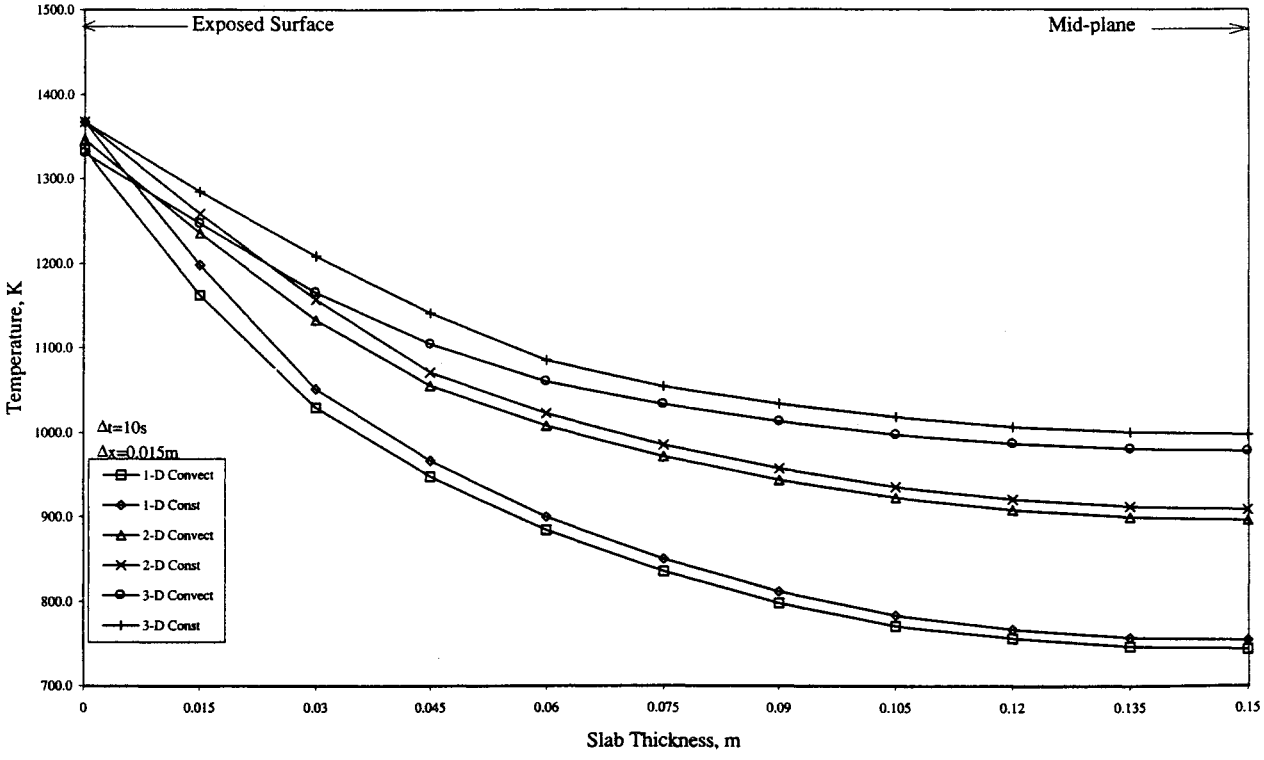

Figure 8. Summary of Variable Properties Results

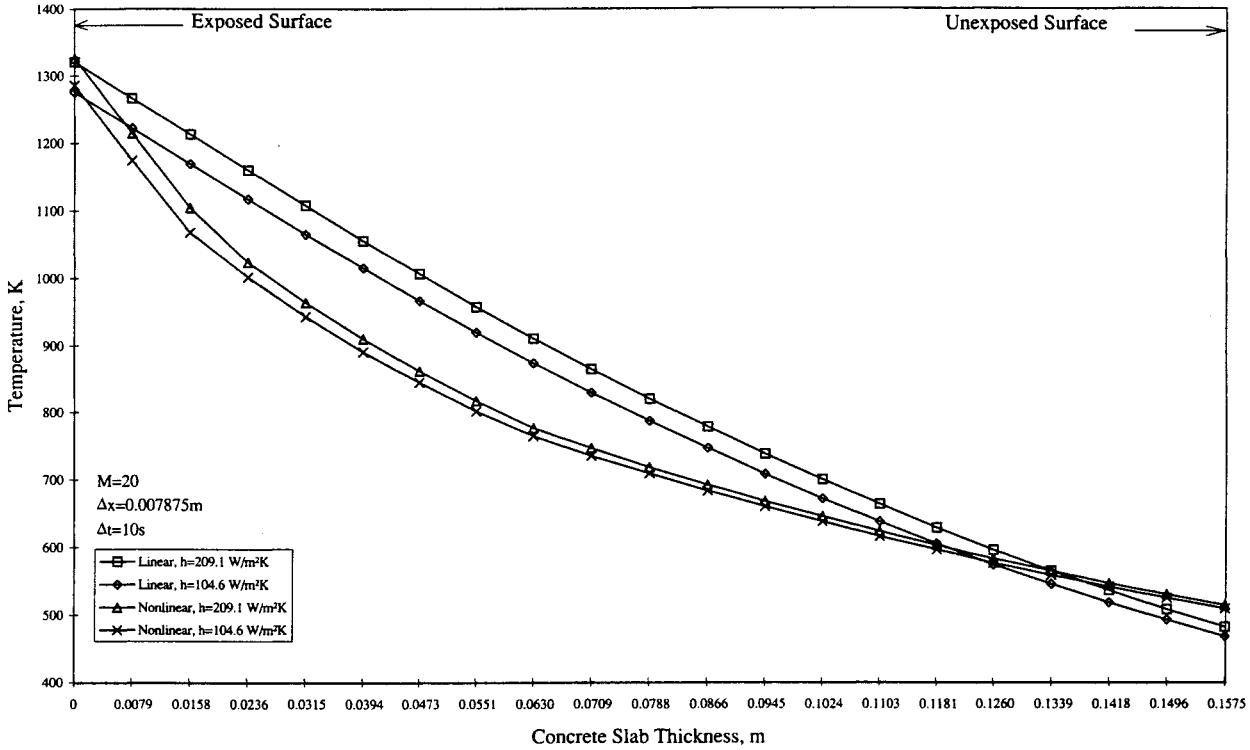

Figure 9. Summary of 1-D ASTM E119/ISO 834 Simulations

Finally, all runs indicate that the unexposed surface temperature is between the upper 400 and 500 K, thereby conservatively over-predicting the maximum allowable temperature (i.e. 433 K) by approximately 50 K. However, it is recognized that the over-prediction would be considerably pared down if the ASTM Temperature-Time Curve has been implemented. For example, at 3 hours, the Curve attains 1325 K, slightly below the constant $T_f = 1366.7$ K adopted here. As a fairly accurate model predicting outcomes of complex or expensive fire tests, the engineering model may not be very useful. Therefore, it needs some enhancement by considering additional physicochemical phenomena. Discussion of these phenomena are beyond the scope of this paper. Nevertheless, it is deemed that as a "crude" or first-order predicting tool for experimental results or for general fire protection engineering practice, this engineering model is acceptable.

Conclusions

A user-friendly or simple numerical procedure has been introduced in this paper. It is expected that most fire professionals can immediately implement the procedure, at least for one-dimensional problems, to simulate fire endurance for some of the simple yet realistic building construction or structural assemblies.

The danger of unconditional adoption of constant flux in lieu of time-varying convective flux for fire (exposed) boundary conditions has been cautioned. Numerical difficulties concerning stability, accuracy and efficiency are briefly discussed. A "correct" approach is introduced to methodically investigate the converging solution which may be disguised among other non-converging but *stable* solutions. The key is to parameterize wide ranges of discretized time steps and lengths (elements or cells). Moreover, numerical performance is discussed in the context of comparing numerical results with analytical solutions of a simple, linear benchmark case. Intrinsic errors do exist in *any* numerical procedure, since it only approximates true and unique solutions.

Easy adaptations for variable thermophysical properties, temporal fire including variational parameters for some of the terms in the combined convective and radiative heat transfer coefficients, heat source or sink, and practical fire damageability studies, have been briefly discussed.

Finally, a practical example simulating one-dimensional fire endurance is demonstrated. Results show that the engineering model is valid for crude or first-order approximations. Since the intent of this introductory paper is to demonstrate a very simple algorithm and to critically discuss its numerical aspects, improvements of the adopted engineering model are not presented here and therefore recommended for future papers.

ACKNOWLEDGEMENTS

The author would like to gratefully thank Mr. Kenneth W. Dungan of HSB Professional Loss Control, Kingston, TN, USA, and Mr. Jesse Beitel of Hughes Associates, Baltimore, MD, USA, for their inspiration and encouragement of this topic.

NOMENCLATURE

English

A	area, m^2 (ft^2)
Bi	Biot (Nusselt) number = hL/k, dimensionless
c	specific heat, J/(kg-K) (Btu/(lb_m-R))
d	diffusion number, dimensionless
Fo	Fourier number = $T_o\alpha/L^2$, dimensionless
G	nonhomogeneous scalar boundary functions, K (R) or W/m^2 (Btu/(s-ft^2))
H	dummy combined convection/radiative heat transfer coefficient, dimensionless
h	heat transfer coefficient, $W/(m^2$-K) (Btu/(s-ft^2-R))
k	thermal conductivity, W/(m-K) (Btu/(s-ft-R))
L	slab thickness, m (ft)
M	total number of discretized elements, cells or control volumes, dimensionless
n	magnitude of outward unit normal vector, m (ft)
q	heat energy, J (Btu)
T	temperature, K (R or°F)
t	time, s
VF	radiative view factor, dimensionless
x,y,z	Cartesian coordinates, m (ft)

Greek

α	thermal diffusivity, m^2/s (ft^2/s)
α_s	absorptivity, dimensionless
ϵ	emissivity, dimensionless
ρ	density, kg/m^3 (lb_m/ft^3)
σ	Stefan-Boltzmann Constant, 5.67E-8 $W/(m^2$-$K^4)$ (4.76E-13 Btu/(s-ft^2-R^4))
Δ	differential, incremental or discretized quantity

Superscripts

•	time rate, 1/s
*	dimensionless quantity
"	per unit area, $1/m^2$ ($1/ft^2$)
...	per unit volume, $1/m^3$ ($1/ft^3$)

Subscripts

cond	conductive
c, conv	convective
ds	differential target surface area
r, rad	radiative
f	fire or exposing fire surface
i,j,k	summation indexes
N	(Neumann) flux boundary condition
n	number of time step or interval
o	reference
p	constant pressure
s	surface
st	heat storage
v	variable thermophysical properties
∞	ambient fluid
x,y,z	Cartesian coordinates

REFERENCES

1. Iding, R.H., Nizamunddin, Z. and Bresler, B., "A Computer Program for the *Fire Res*ponse of Structures—*T*hermal *Three*-Dimensional Version," The University of California, Berkeley, Civil Engineering Department, Berkeley, CA, USA, October 1977.

2. Tien, C.L., Lee, K.Y. and Stretton, A.J., "Radiation Heat Transfer," *Fire Protection Engineering Handbook*, 2nd Ed., pp. 1-73–1-75, Society of Fire Protection Engineers/National Fire Protection Association, Boston, MA, USA, 1995.

3. Babrauskas, V., "Pool Fires: Burning Rates and Heat Fluxes," *Fire Protection Handbook*, 16th Ed., National Fire Protection Association, Quincy, MA, USA, p. 21–41, 1986.

4. Incroppera, F.P. and Dewitt, D.P., *Fundamentals of Heat Transfer*, Wiley, p. 773, 1981.

5. Hoffmann, K.A. and Chiang, S.T., *Computational Fluid Dynamics for Engineers – Volume I*, pp. 126–152, Engineering Education System™ Wichita, KS, USA, 1993.

6. Shih, T.M., *Numerical Heat Transfer*, Hemisphere, pp. 136–172, 1984.

7. Baker, A.J., *Finite Element Computational Fluid Mechanics*, Hemisphere, pp. 186–195, 1985.

8. Baker, A.J. and Pepper, D.W., *Finite Elements 1-2-3*, pp. 79–88, McGraw Hill, 1991.

9. Gross, D., *NBSIR 85-3223 Data Sources for Parameters Used in Predictive Modeling of Fire Growth and Smoke Spread*, p. 10, National Institute of Standards and Technology, Gaithersburg, MD, USA, Sept. 1985.

10. Fleischmann, C., "Analytical Methods for Determining Fire Resistance of Concrete Members," *Fire Protection Engineering Handbook*, 2nd Ed., p. 4–205, Society of Fire Protection Engineers/National Fire Protection Association, Boston, MA, USA, 1995.

11. *Fire Test Standards – ASTM E 119 (88) – Standard Test Methods for Fire Tests of Building Construction and Materials*, p. 519, American Society for Testing and Materials, Philadelphia, PA, USA, 1990.